Nanotubes from Isomeric Dibenzoylmethane Molecules

Liyun Zhao,[a] Wensheng Yang,[b] Yi Luo,[c] Tianyou Zhai,[a] Guangjin Zhang,[a] and Jiannian Yao*[a]

Abstract: Organic nanotubes of various diameters were fabricated from the isomeric molecule dibenzoylmethane (DBM) by using an immersing technique with ordered porous alumina membrane as the template. The ratio of the enol isomers of DBM increased as the diameters of the nanotubes decreased. In addition, although almost no fluorescence could be detected for the DBM monomer, a striking enhancement in the fluorescence emission intensity of the nanotubes was observed as the diameters decreased. This is due to the increased ratio of the enol isomers.

Keywords: enols · fluorescence · isomers · nanotubes · template synthesis

Introduction

Since the discovery of carbon nanotubes,[1,2] considerable attention has been directed towards nanotubular structures on account of their unique physicochemical and electronic properties, and also because of their potential applications in various fields, such as electronics, optics, catalysis, energy storage, and biological systems.[3–9] Recently, the number of studies on organic nanotubes (ONTs) has increased, however, most of these have focussed on nanotubes of polymers, such as polypyrrole, polyaniline, poly(methyl methacrylate) (PMMA), and polystyrene.[10–12] Although research concerning organic nanotubes of low molecular weight active compounds is still in its infancy, several systems have been developed by employing the self-assembly and template-based methods.[13–20] In organic molecular crystals, the electronic and optical properties are fundamentally different from those of inorganic crystals, due to the weak intermolecular interactions of the van der Waals type or the hydrogen bond.[21,22] This may result in phenomena that contrast to those of strongly bonded nanotubes of metals and semiconductors. According to earlier work, organic nanoparticles exhibit size-dependent optical properties that arise from, for example, the aggregation effect, surface effect, or the increased intermolecular interactions induced by the change of lattice.[21–23] Molecules within tubular structures may be arranged differently from those in particles, which might also account for some unusual properties. The size effect of organic nanotubes is, therefore, of great interest.

β-Diketones have always been of interest to inorganic, organic, and physical chemists, due to their isomeric keto–enol interconversion, which is fundamental to many organic synthetic pathways, biochemical processes, and enzymatic mechanisms.[24,25] One such molecule is dibenzoylmethane (DBM, Scheme 1), a UV absorber and photostablizer widely used in the protection of polymer materials, and a conventional chelate to detect trace metal ions by fluorescence measurement. In addition, due to its oral bioavailability and low toxicity, DBM is biologically relevant as a chemopreventative blocking agent in the treatment of breast cancer, and has the potential to reverse ischemic diseases by induc-

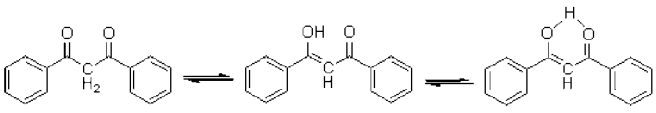

Scheme 1. Equilibrium showing the keto–enol isomerism of DBM molecules.

[a] Dr. L. Zhao, Dr. T. Zhai, Dr. G. Zhang, Prof. J. Yao
Key Laboratory of Photochemistry, Center for Molecular Science
Institute of Chemistry, Chinese Academy of Sciences
Beijing 100080 (P. R. China)
Fax: (+86) 10-826-16517
E-mail: jnyao@iccas.ac.cn

[b] Prof. W. Yang
Present address: College of Chemistry, Jilin University
Changchun 130023 (P. R. China)

[c] Prof. Y. Luo
Theoretical Chemistry, Royal Institute of Technology
AlbaNova University Center, 10691 Stockholm (Sweden)

 DOI: 10.1002/chem.200401265

ing angiogenesis in vivo.[26–28] Here, we describe the size-dependent properties of DBM nanotubes of different diameters, synthesized by using the immersing technique with porous alumina membrane as the template. The ratio of the enol isomers increased as the diameters of the nanotubes decreased. Preferential orientations of DBM molecules in the nanotubular structures were detected. In addition, the nanotubes exhibited enhanced photoluminescence as their diameter decreased, whereby the DBM monomer was almost nonfluorescent.

Results and Discussion

Use of the simple immersing technique with porous alumina membrane as the template is a facile route to the fabrication of organic nanotubes.[18,29] The diameter, length, and wall thickness of the nanotubes can be well controlled by the choice of template. We prepared DBM nanotubes by repeatedly immersing the porous alumina membrane into the nearly saturated diethyl ether solution of DBM, and then evaporating the solvent at intervals. The typical top-view images of the DBM nanotubes after complete removal of the template (Figure 1a–c) reveal that the nanotubes are arranged in a continuous, parallel, and well-ordered manner, with uniform diameters and wall thicknesses. The low magnification image (Figure 1c) indicates clearly that the diameters and lengths of the nanotubes correspond well with the diameter of the membrane pores and the thickness of the template used and no tubes grew from the surface of the template. DBM nanotubes of different sizes were prepared by using alumina template with different pore diameters. The field emission scanning electron microscope (FESEM) images in Figure 1a and b show nanotubes of diameters 100 and 200 nm, respectively, as a representative sample. By imaging different regions of the materials, the nanotubes were determined to be hollow throughout their entire length, with uniform wall thickness. As shown in the cross-sectional image (Figure 1d), the open tips of the tubes were clearly displayed. By bending the template and then etching away aluminum oxide with aqueous sodium hydroxide, some tubes were slightly tilted and broken in the middle to show the open tips. It is proposed that the capillary effect is favorable for the nucleation and growth of the nanotubes in the inner surface of the pores of the membrane, based on the "layer-by-layer" mechanism.[18,29]

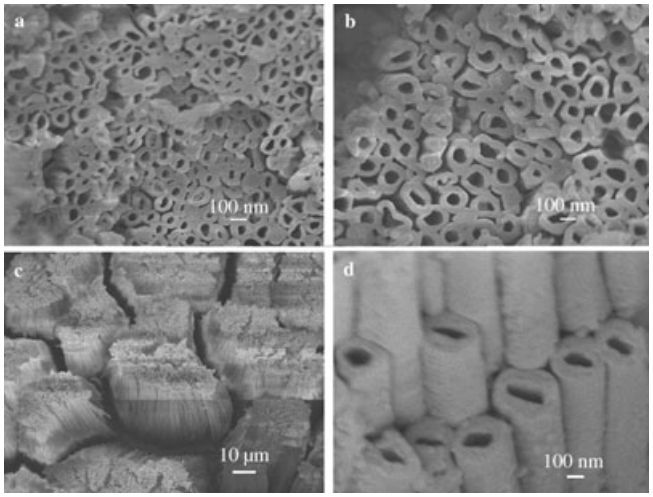

Figure 1. FESEM images of the DBM nanotubes prepared after the complete removal of the template by alkaline treatment: typical top view of nanotubes with diameters of a) 100 nm and b) 200 nm; c) low magnification of nanotubes with diameters of 200 nm; d) cross-sectional view of nanotubes with diameters of 200 nm.

X-ray diffraction (XRD) measurements were recorded to probe the internal structure of the nanotubes (Figure 2), and to give information about their possible stoichometry. The diffraction peaks of DBM nanotubes and DBM powder are clearly distinguishable and can be perfectly indexed to the orthorhombic crystal structure of DBM (JCPDS card No.32–1641). Specifically, in the spectra of DBM nanotubes with different diameters, there is a very sharp diffraction peak at $2\theta = 16.4°$, corresponding to the (200) plane of the orthorhombic DBM, and all other diffraction peaks are either very weak or undetectable. This result indicates that DBM molecules prefer to arrange themselves within the nanotubes along the (200) plane.

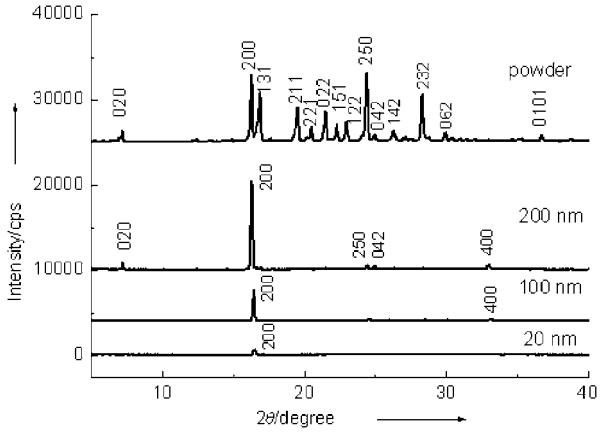

Figure 2. XRD patterns of DBM nanotubes with diameters of 20, 100, and 200 nm, and that of DBM powder.

The DBM molecule is a typical β-diketone that can exist as a keto isomer, and as enol isomers with and without intramolecular hydrogen bonds (Scheme 1). To characterize further the state of the molecules in the nanotubes, the optimized geometry of the different isomers of DBM was determined (Figure 3). The energies of the keto isomer and the enol isomer without intramolecular hydrogen bonding (enol-n) are 7.2 and 17.7 kcal mol^{-1} greater, respectively, than that of the enol isomer with the intramolecular hydrogen bond (enol-hb). The enol-hb isomer is probably dominant in an isolated system, and both the keto and enol-hb

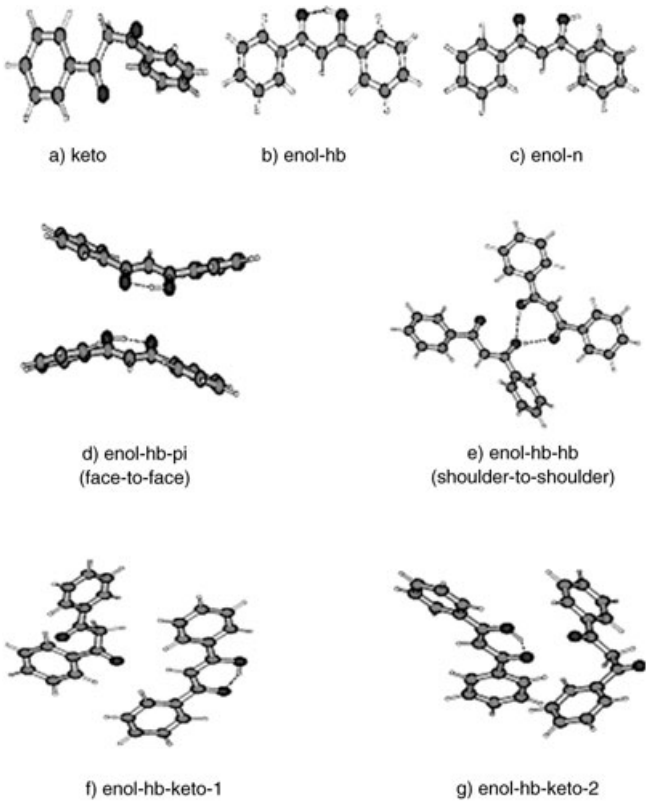

Figure 3. Structures of DBM: a) keto isomer; b) enol isomer with intramolecular hydrogen bonding; c) enol isomer without intramolecular hydrogen bonding; d) enol-hb dimer in the π-π stacking mode (face-to-face); e) enol-hb dimer in the hydrogen-bonging stacking mode (shoulder-to-shoulder); f) keto and enol-hb dimer without the face-to-face arrangement of oxygen atoms; and g) keto and enol-hb dimer with the face-to-face arrangement of oxygen atoms.

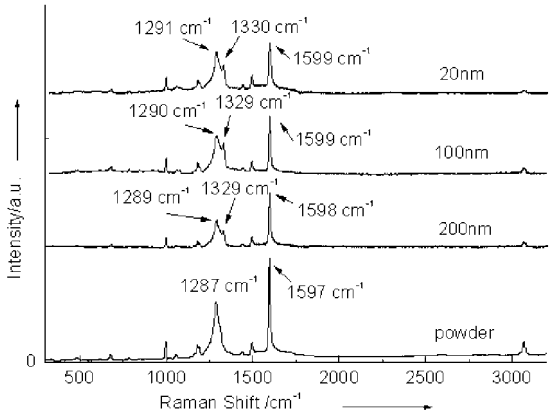

Figure 4. Raman spectra of DBM nanotubes with diameters of 20, 100, and 200 nm, and that of DBM powder.

isomers can be expected in the condensed phase. Based on this assumption, a series of dimer structures of DBM molecules were optimized. Four representative dimers are shown in Figure 3d–g; the enol-hb dimer in the π-π stacking mode (enol-hb-pi), the enol-hb dimer in the hydrogen-bonding mode (enol-hb-hb), and the keto and enol-hb dimers in two different, mutual positions: with (enol-hb-keto-2) and without (enol-hb-keto-1) the face-to-face arrangement of oxygen atoms. Notably, the enol-n isomer is unlikely to exist in the dimer system, because the geometry optimization always favors the enol-hb isomer at the end of minimization. The energies of the dimeric structures of enol-hb-keto-1, enol-hb-keto-2, and enol-hb-hb are 3.88, 5.97, and 15.7 kcal mol^{-1} higher, respectively, than that of the enol-hb-pi dimer, which has the lowest energy.

Raman spectra were recorded to help elucidate the internal structure of the nanotubes (Figure 4). The characteristic peaks of DBM molecules[30–32] were observed at around 3000, 1600, 1500, 1450, and 1260 cm^{-1} in both the nanotubes and the powder, which confirms the composition of the nanotubes. The spectra of DBM nanotubes resemble that of the powder, except for the peaks in the region of ~1200–1380 cm^{-1}. In the case of the powder, the predominant peak is the one centered at 1287 cm^{-1}, whereas the spectra of DBM nanotubes show two distinguishable peaks centered at approximately 1290 and 1329 cm^{-1}. In addition, the intensity of the new peak at 1329 cm^{-1} increased as the sizes of the nanotubes decreased. This new peak is probably an indicator of the structural differences between the nanotubes and the powder, as well as the size-dependent character of the nanotubes.

The Raman spectra of the keto isomer, the enol isomers, and the proposed dimers of DBM (see Figure 3) were calculated to help explain the experimental results (Figure 5). Comparison of the spectra of the enol isomers with (DBM-enol-hb) and without (DBM-enol-n) intramolecular hydrogen bonds shows that the wag-motion of the OH group at 1326 cm^{-1} seems to be related to the existence of hydrogen bonding (Figure 5a). From the calculated Raman spectra of the four dimers (Figure 3d–g), the existence of the enol-hb-hb dimer (Figure 3e), which should show a characteristic peak at 2858 cm^{-1} (Figure 5b) corresponding to the hydrogen-bonding network OH···OH···O, could be excluded in both the nanotubes and powder of DBM, due to its absence in experimental observations (Figure 4). There is no significant difference among the calculated Raman spectra of the enol-hb-pi dimer, the enol-hb monomer, and the enol-hb-keto dimer. Based on the experimental results, the enol-hb isomer in the face-to-face stacking manner, and the mixtures of the enol-hb and keto isomers are the possible components of the nanotubes. The distinctly increased intensity of the peak at around 1329 cm^{-1} may be related to the incremental hydrogen bonding, attributable to the decreasing size of the nanotubes.

The X-ray photoelectron spectroscopy (XPS) spectra in Figure 6 show the C_{1s} peaks for the DBM nanotubes of diameters 20, 100, and 200 nm, and that of the DBM powder. The main asymmetric peaks are all centered at around 284.6 eV, with a long tail extending to the higher energy region of the spectra. The peaks can be well fitted by three

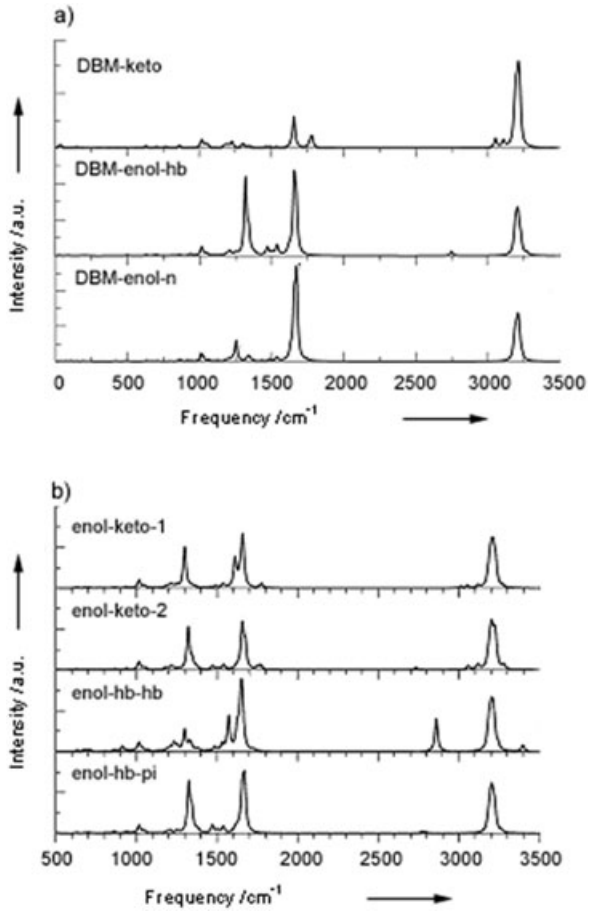

Figure 5. Calculated Raman spectra of: a) DBM monomers in different isomers of keto and enol with and without intramolecular hydrogen bonds; b) DBM dimers of enol-keto-1 (keto and enol-hb dimer without the face-to-face arrangement of oxygen atoms), enol-keto-2 (keto and enol-hb dimer with the face-to-face arrangement of oxygen atoms), enol-hb-hb (dimer of enol-hb in the shoulder-to-shoulder stacking mode), and enol-hb-pi (dimer of enol-hb in the face-to-face stacking mode).

peaks representing C−C (C=C) (284.6 eV), C−O (286.4 eV), and C=O (288.7 eV), respectively.[33–34]

Calculated XPS spectra of the enol-hb and keto monomers and dimers are shown in Figure 7. The spectra of the monomers show two distinct spectral features; a strong peak from carbon bonds on the phenyl ring, and a weak peak from either C=O or C−OH bonds. The two peaks of the enol-hb isomer are located at 284.8 and 286.7 eV, which are in close agreement with the corresponding experimental spectral features. The C=O bond of the keto monomer contributes a weak spectral feature at around 287.3 eV, which is about 1.4 eV lower than that of the C=O bond observed experimentally (288.7 eV, Figure 6). This difference is greater than the accuracy of the DFT method used for calculating XPS spectra.[35–36] Such a large deviation is probably induced by the intermolecular interactions in the nanotubes. To test this assumption, the C_{1s} binding energies of two dimers were calculated (Figure 7). Although the interaction between the keto and enol-hb monomers has no effect on the C_{1s} binding energy of the enol-hb dimer, it clearly affects that of the keto dimer. The interaction results in the broadening of the C_{1s} peak of the C=O bond. Thus, it appears that the C=O bonds are quite sensitive to their surroundings, although the binding energies for the models adopted in Figure 7 are not in good agreement with the experimental results. However, it is clear that the ratio between the weak peaks of C=O (keto) at 288.7 eV and C−O (enol-hb) at 286.4 eV is related to the content of different isomers. From the XPS spectra, the ratios of the peaks of C−O to C=O were calculated to be 3.1, 2.6, and 2.2 for the 20, 100, and 200 nm DBM nanotubes, respectively, and 1.6 for the DBM powder. In other words, the ratio of the enol isomers increases as the diameters of the nanotubes decreases.

Although the DBM monomer is almost nonfluorescent, the DBM nanotubes showed enhanced fluorescence emissions (Figure 8). For the nanotubes with diameters of 20, 100, and 200 nm, the photoluminescence intensities were 6.4, 3.2, and 1.3 times that of the powder, respectively. Such a striking enhancement of the photoluminescence of the powder and nanotubes compared to that of the monomer may be attributable to the aggregation effect, surface effect, or the increased intermolecular interaction induced by the lattice change in the nanotubes. The clear bathochromic shifts in the emissions of the nanotubes and powder compared to that of the dilute solution suggest the formation of face-to-face excimers in the nanotubes and powder. The further bathochromic shift of the nanotubes compared to that of the powder shows that there should be a slight difference between them in the degree of aggregation. The enhanced planarity and rigidity of the molecules resulting from the intramolecular hydrogen bonds in the enol-hb isomer, especially those in the π-π stacking manner, will be profitable to the aggregation-induced emission process.[37–38] Thus, as their diameters decrease, the nanotubes exhibit enhanced emission due to the increased ratio of enol isomers. The intermolecular hydrogen bonding among the enol and keto isomers may also contribute to the size-dependent emission.

Conclusion

We have successfully fabricated DBM nanotubes of different sizes by using the immersing technique with porous alumina membrane as the template. DBM molecules oriented preferentially along the (200) plane of the crystal, and the ratio of enol isomers increased as the size of the nanotubes decreased. Furthermore, the smaller the diameter of the DBM nanotubes, the greater the fluorescence emissions observed, with DBM almost nonfluorescent in the monomer state. These results should help to progress the study of functional organic nanotubes that have potential applications in fields such as optical devices, sensors, and biotechnology.

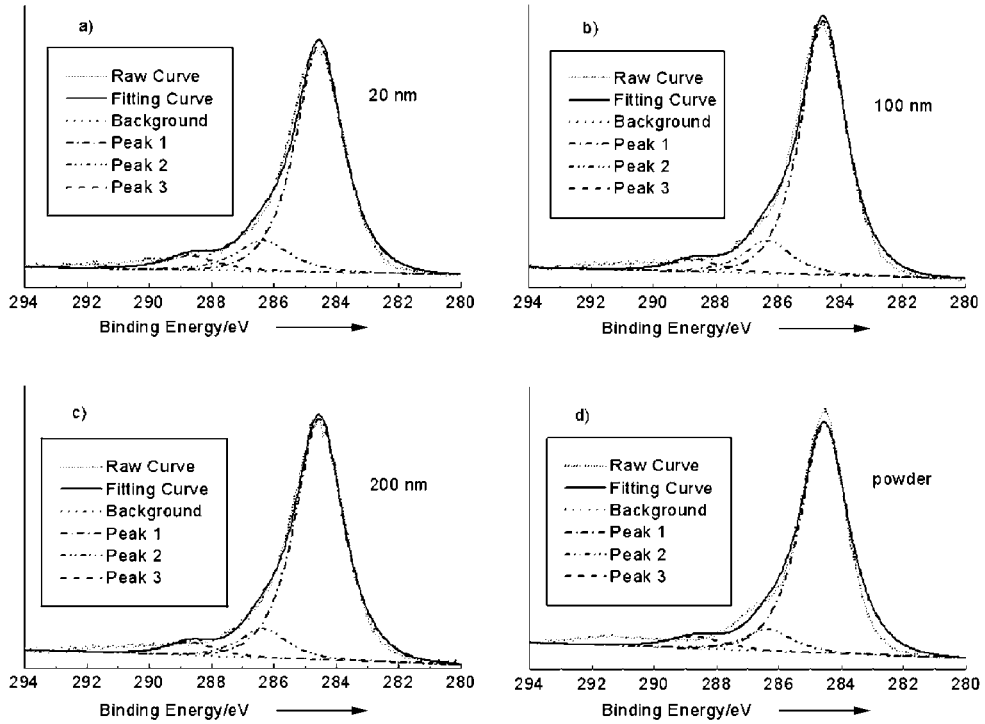

Figure 6. C_{1s} XPS spectra of DBM nanotubes with diameters of a) 20 nm, b) 100 nm, and c) 200 nm. d) XPS spectra of the powder.

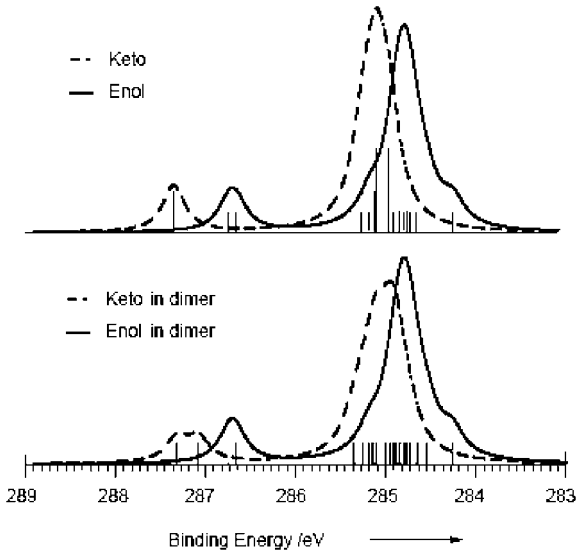

Figure 7. Calculated XPS spectra of different DBM isomers and their dimers.

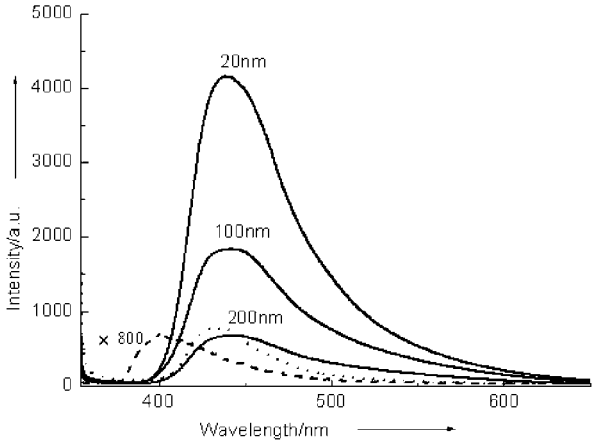

Figure 8. Photoluminescence spectra of (——) DBM nanotubes with diameters of 20, 100, and 200 nm; (•••••) DBM powder; and (– – –) a chloroform solution of DBM (2.6×10^{-4} M) with multiplying treatment. The excitation wavelength was 344 nm.

Experimental Section

Materials: Dibenzoylmethane (DBM, +99%) was purchased from ACROS and was used without further purification. Purified water was obtained by passing distilled water through a Milli-Q water purification system (Millipore), and had a resistivity of 18.2 MΩ·cm^{-1}. The commercially available membrane filter (Whatman, Anodisc 13) with quoted pore diameters of 20, 100, and 200 nm was used as the template.

Methods: The DBM nanotubes were prepared by using the immersing technique with porous alumina membrane as the template as follows. Porous alumina templates were ultrasonically treated with solvents of different polarity (water, ethanol, acetone, for 15 min, and diethyl ether for 5 min), followed by annealing at 100 °C for 1 h. The purpose of the treatment was to eliminate the bubbles in the pores of the membrane and to improve wetting of the membrane by the DBM solution. The pretreated template was then immersed in the nearly saturated solution of DBM in diethyl ether for about 2 min, then removed to allow the solvent to air-dry completely. The above procedure was repeated for 20 cycles. Finally, the surface layer of the template was removed by polishing it with 1500 grid sandpaper to enable further characterization and detection.

The morphologies and sizes of the nanotubes were observed by using a field emission scanning electron microscope (FESEM, JSM-6700F, JEOL) operating at an accelerating voltage of 3 kV. Specimens for FESEM were prepared as follows. After removing the surface layer of

the template, the sample was fixed to a piece of copper tape and soaked in 6 M aqueous NaOH for 1 h to remove the alumina template completely. It was then rinsed carefully with purified water several times. The tape was then attached to an FESEM stub, and was then sputtered with a layer of platinum by using a current of 5 mA and a pressure of 3 mmHg, to prevent charging during SEM imaging.

X-ray diffraction (XRD) measurements were performed by using a Rigaku X-Ray Diffractometer (D/max-2400) with an X-ray source of $Cu_{K\alpha}$ ($\lambda = 1.5406$ Å) at 40 kV and 120 mA, at a scan rate of 0.02° (2θ) per 0.12 s. The Raman spectra were recorded in the backscattering geometry by using a Renishaw-2000 Raman spectrometer with the 514.5 nm line of an Ar ion laser as the excitation source. To avoid destroying the structure of the nanotubes, a low laser power of 5 mW was used. XPS spectra were recorded by using an ESCALab 200i-XL spectrometer (VG Scientific). The photoluminescence (PL) spectra were measured by using a Hitachi F-4500 fluorescence spectrophotometer with excitation and emission slits of 5/5 nm.

The geometries of the DBM molecules were optimized at a hybrid density functional B3LYP level with a 6–31G(d,p) basis set. All Raman spectra were calculated at the same level as those for geometry by using the Gaussian 98 program.[39] The XPS spectra of DBM molecules were calculated by using gradient correct density functional theory (DFT), as implemented in the DeMon code.[40] The PD86 correlation functional by Perdew and Wang[41] and the exchange functional of Becke[42] were used to calculate the ionization potentials (IP) of all carbon atoms, for which the difference in energy between the ground state and the core hole state is computed. We have used the igloo-iii triple zeta basis of Kutzelnigg, Fleischer, and Schindler[43] to describe the core-excited carbon atoms, and four-electron effective core potentials (ECP) for the remaining carbon atoms. The rest elements are described by a 6–31G(d,p) basis set.

Acknowledgements

This work was supported by the National Natural Science Foundation of China (No.50221201, 90301010, 20373077, 20471062), the Chinese Academy of Sciences, and the National Research Fund for Fundamental Key Projects No.973. Y.L. acknowledges the support of the Swedish Research Council (VR).

[1] A. Oberlin, M. Endo, T. Koyama, *J. Cryst. Growth* **1976**, *32*, 335–349.
[2] S. Iijima, *Nature* **1991**, *354*, 56.
[3] J. Hu, T. W. Odom, C. M. Lieber, *Acc. Chem. Res.* **1999**, *32*, 435.
[4] G. Che, B. B. Lakshmi, E. R. Fisher, C. R. Martin, *Nature* **1998**, *393*, 346.
[5] K. B. Jirage, J. C. Hulteen, C. R. Martin, *Science* **1997**, *278*, 655.
[6] S. B. Lee, D. T. Mitchell, L. Trofin, T. K. Nevanen, H. Söderlund, C. R. Martin, *Science* **2002**, *296*, 2198.
[7] P. G. Collins, A. Zettl, H. Bando, A. Thess, R. E. Smalley, *Science* **1997**, *278*, 100.
[8] D. T. Mitchell, S. B. Lee, L. Trofin, N. Li, T. K. Nevanen, H. Söderlund, C. R. Martin, *J. Am. Chem. Soc.* **2002**, *124*, 11864.
[9] Y. Xia, P. Yang, Y. Sun, Y. Wu, B. Mayers, B. Gates, Y. Yin, F. Kim, H. Yan, *Adv. Mater.* **2003**, *15*, 353.
[10] C. R. Martin, *Science* **1994**, *266*, 1961.
[11] C. Jérôme, S. Demoustier-Champagne, R. Legras, R. Jérôme, *Chem. Eur. J.* **2000**, *6*, 3089.
[12] M. Steinhart, J. H. Wendorff, A. Greiner, R. B. Wehrspohn, K. Nielsch, J. Schilling, J. Choi, U. Gösele, *Science* **2002**, *296*, 1997.
[13] M. R. Ghadiri, J. R. Granja, R. A. Milligan, D. E. McRee, N. Khazanovich, *Nature* **1993**, *366*, 324.
[14] M. R. Ghadiri, J. R. Granja, L. K. Buehler, *Nature* **1994**, *369*, 301.
[15] J. M. Schnur, *Science* **1993**, *262*, 1669.
[16] A. Harada, J. Li, M. Kamachi, *Nature* **1993**, *364*, 516.
[17] D. T. Bong, T. D. Clark, J. R. Granja, M. R. Ghadiri, *Angew. Chem.* **2001**, *113*, 1016; *Angew. Chem. Int. Ed.* **2001**, *40*, 988.
[18] L. Y. Zhao, W. S. Yang, Y. Ma, J. N. Yao, Y. L. Li, H. B. Liu, *Chem. Commun.* **2003**, 2442.
[19] K. Lu, J. Jacob, P. Thiyagarajan, V. P. Conticello, D. G. Lynn, *J. Am. Chem. Soc.* **2003**, *125*, 6391.
[20] J. H. Jung, S.-H. Lee, J. S. Yoo, K. Yoshida, T. Shimizu, S. Shinkai, *Chem. Eur. J.* **2003**, *9*, 5307.
[21] H. B. Fu, J. N. Yao, *J. Am. Chem. Soc.* **2001**, *123*, 1434.
[22] H. B. Fu, B. H. Loo, D. B. Xiao, R. M. Xie, X. H. Ji, J. N. Yao, B. W. Zhang, L. Q. Zhang, *Angew. Chem.* **2002**, *114*, 1004; *Angew. Chem. Int. Ed.* **2002**, *41*, 961.
[23] D. B. Xiao, L. Xi, W. S. Yang, H. B. Fu, Z. G. Shuai, Y. Fang, J. N. Yao, *J. Am. Chem. Soc.* **2003**, *125*, 6740.
[24] J. Emsley, *Struct. Bonding (Berlin)* **1984**, *57*, 147.
[25] G. Gilli, F. Bellucci, V. Ferretti, V. Bertolasi, *J. Am. Chem. Soc.* **1989**, *111*, 1023.
[26] K. Singletary, C. MacDonald, M. Iovinelli, C. Fisher, M. Wallig, *Carcinogenesis* **1998**, *19*, 1039.
[27] N. J. Mabjeesh, M. T. Willard, W. B. Harris, H. Y. Sun, R. Wang, H. Zhong, J. N. Umbreit, J. W. Simons, *Biochem. Biophys. Res. Commun.* **2003**, *303*, 279.
[28] M. T. Huang, Y. R. Lou, J. G. Xie, W. Ma, Y. P. Lu, P. Yen, B. T. Zhu, H. Newmark, C. T. Ho, *Carcinogenesis* **1998**, *19*, 1697.
[29] H. Liu, Y. Li, L. Jiang, H. Luo, S. Xiao, H. Fang, H. Li, D. Zhu, D. Yu, J. Xu, B. Xiang, *J. Am. Chem. Soc.* **2002**, *124*, 13370.
[30] R. S. Rasmussen, D. D. Tunnicliff, R. R. Brattain, *J. Am. Chem. Soc.* **1949**, *71*, 1068.
[31] F. T. Wall, W. F. Claussen, *J. Am. Chem. Soc.* **1939**, *61*, 2812.
[32] N. B. Colthup, L. H. Daly, S. E. Wiberley, *Introduction to Infrared and Raman Spectroscopy*, Academic Press, **1964**, pp. 245.
[33] C. D. Wagner, W. M. Riggs, L. E. Davis, J. F. Moulder, G. E. Muilenberg, *Handbook of X-ray Photoelectron Spectroscopy*, Perkin–Elmer Coorporation, Minnesota (USA), **1978**.
[34] H. Pan, L. Liu, Z. X. Guo, L. Dai, F. Zhang, D. Zhu, R. Czerw, D. L. Carroll, *Nano Lett.* **2003**, *3*, 29.
[35] G. Cavigliasso, D. P. Chong, *J. Chem. Phys.* **1999**, *111*, 9485.
[36] L. Triguero, O. Plashkevych, L. G. M. Pettersson, H. Ågren, *J. Electron Spectrosc. Relat. Phenom.* **1999**, *104*, 195.
[37] S. Y. Ryu, S. Kim, J. Seo, Y.-W. Kim, O.-H. Kwon, D.-J. Jang, S. Y. Park, *Chem. Commun.* **2004**, *1*, 70.
[38] J. Chen, C. C. W. Law, J. W. Y. Lam, Y. Dong, S. M. F. Lo, I. D. Williams, D. Zhu, B. Z. Tang, *Chem. Mater.* **2003**, *15*, 1535.
[39] Gaussian 98 (Revision A.9), M. J. Frisch, G. W. Trucks, H. B. Schlegel, G. E. Scuseria, M. A. Robb, J. R. Cheeseman, V. G. Zakrzewski, J. A. Montgomery, R. E. Stratmann, J. C. Burant, S. Dapprich, J. M. Millam, A. D. Daniels, K. N. Kudin, M. C. Strain, O. Farkas, J. Tomasi, V. Barone, M. Cossi, R. Cammi, B. Mennucci, C. Pomelli, C. Adamo, S. Clifford, J. Ochterski, G. A. Petersson, P. Y. Ayala, Q. Cui, K. Morokuma, D. K. Malick, A. D. Rabuck, K. Raghavachari, J. B. Foresman, J. Cioslowski, J. V. Ortiz, B. B. Stefanov, G. Liu, A. Liashenko, P. Piskorz, I. Komaromi, R. Gomperts, R. L. Martin, D. J. Fox, T. Keith, M. A. Al-Laham, C. Y. Peng, A. Nanayakkara, C. Gonzalez, M. Challacombe, P. M. W. Gill, B. G. Johnson, W. Chen, M. W. Wong, J. L. Andres, M. Head-Gordon, E. S. Replogle, J. A. Pople, Gaussian, Inc., Pittsburgh, PA, **1998**.
[40] DEMON-KS Version 4.0, M. E. Casida, C. Daul, A. Goursot, A. Koester, L. G. M. Pettersson, E. Proynov, A. St-Amant, D. R. Salahub principal authors, H. Duarte, N. Godbout, J. Guan, C. Jamorski, M. Leboeuf, V. Malkin, O. Malkina, M. Nyberg, L. Pedocchi, F. Sim, L. Triguero, A. Vela contributing authors, deMon Software, **1997**.
[41] J. P. Perdew, Y. Wang, *Phys. Rev. B* **1986**, *33*, 8822.
[42] A. D. Becke, *Phys. Rev. A* **1988**, *38*, 3098.
[43] W. Kutzelnigg, U. Fleischer, M. Schindler, *NMR Basic Principles and Progress, Volume 23*, Springer, Heidelberg, **1990**.

Received: December 9, 2004
Published online: April 13, 2005